



Angiotensin Type 2 Receptor Pharmacological Agonist Relieves Neurocognitive Deficits via Reducing Neuroinflammation and Microglial Engulfment of Dendritic Spines

Liang Shen¹ · Dan-yang Chen² · Qian-qian Lou² · Peng Cao² · Rui Hu² · Yan Jin² · Di Wang^{1,3} · Shan-shan Hu⁴

Received: 14 July 2022 / Accepted: 8 November 2022

© The Author(s), under exclusive licence to Springer Science+Business Media, LLC, part of Springer Nature 2022

Abstract

Mechanically ventilated patients suffering critical illness are at high risk of developing neurocognitive impairments. Angiotensin type 2 receptor (AGTR2) has been demonstrated to be anti-inflammatory and neuroprotective. The present study thus aimed to investigate whether AGTR2 can alleviate cerebral dysfunction in mice subjected to cochallenge with lipopolysaccharide (LPS) and mechanical ventilation (MV), and to reveal the underlying mechanism. We utilized a mice model that received a single injection of LPS (1 mg/kg, intraperitoneally) followed 2 h later by MV (10 ml/kg, lasting for 2 h). Pretreatment with the AGTR2 pharmacological agonist C21 (0.03, 0.3, and 3 mg/kg, intraperitoneally, once daily, lasting for 10 days). Locomotor activity and behavioral deficits were evaluated 24 h post-MV by open-field and fear-condition tests. Brain hippocampus and prefrontal cortex tissues were collected for immunofluorescence staining and western blotting to evaluate the resulting impacts on microglia, including morphological traits, functional markers, synaptic engulfment, superoxide production, and signaling molecules. Compared with vehicle-control, pre-administrated C21 reduced the branch endpoints and length of microglia processes in a dose-dependent manner in mice subjected to LPS/MV. The neuroprotective effect of AGTR2 was behaviorally confirmed by the improvement of memory decline in LPS/MV-treated mice following C21 pretreatment. In addition to morphological alterations, C21 reduced microglial functional markers and reduced microglial-dendrite contact and microglial engulfment of synaptic protein markers. In terms of the underlying molecular mechanism, AGTR2 stimulation by C21 leads to activation of protein phosphatase 2A, which subsequently mitigates microglial PKC δ and NF- κ B activation, and inhibits NOX2-derived ROS production. The AGTR2 agonist C21 alleviates behavioral deficits in those mice subjected to LPS/MV, via mechanisms that involve reactive microglia and abnormal synaptic plasticity in NOX2-derived ROS and the PKC δ -NF κ B pathway.

Keywords Neurocognitive disturbances · Mechanical ventilation · Systemic inflammation · Microglia · Synaptic engulfment · Oxidative stress · AGTR2

Abbreviations

MV Mechanical ventilation
AGTR2 Angiotensin type 2 receptor

ICUs Intensive care units
SAE Sepsis-associated encephalopathy
CNS Central nervous system
LPS Lipopolysaccharide
NOX2 NADPH oxidase 2
ANOVA Analysis of variance

Liang Shen, Dan-yang Chen, and Qian-qian Lou these authors have contributed equally to this work and share first authorship.

✉ Shan-shan Hu
shanshanhu@ahmu.edu.cn

¹ Anhui Provincial Hospita, Anhui Provincial Hospital Affiliated to Anhui Medical University, Anhui Medical University, Hefei 230036, China

² Department of Neurobiology, Division of Life Sciences and Medicine, University of Science and Technology of China, Hefei 230001, China

³ Department of Anesthesiology, First Affiliated Hospital of USTC (Anhui Provincial Hospita), Division of Life Sciences and Medicine, University of Science and Technology of China (USTC), Hefei 230001, China

⁴ Department of Clinical Laboratory, First Affiliated Hospital of USTC (Anhui Provincial Hospita), Division of Life Sciences and Medicine, University of Science and Technology of China (USTC), Hefei 230001, China

ROS	Oxygen species
C21	Compound 21
OFT	Open field test
FCT	Fear Conditioning test
ox-DHE	Oxidized dihydroethidine

Introduction

Cerebral dysfunction ranging from acute delirium to long-term neurocognitive impairment may occur among up to 80% of critically ill patients after intensive care unit (ICU) discharge (Pandharipande et al. 2013; Sasannejad et al. 2019). During the COVID-19 pandemic, this problem has been particularly emphasized in severe coronavirus-infected patients who were admitted to ICUs and received life-saving support (Helms et al. 2020; Pun et al. 2021). Considerable progress has been made in delineating the pathophysiological mechanism that underlies the concomitant neurocognitive disorder. Some risk factors have been identified, such as systemic inflammation and mechanical ventilation (MV), which have both independently been shown to be associated with cerebral dysfunction in patients surviving critical illness (Wilcox et al. 2013). Sepsis, a lethal syndrome characterized by a systemic inflammation that develops in response to the infection, is the most common reason for ICU stay and is associated with a high prevalence of cerebral dysfunction termed sepsis-associated encephalopathy (Gofton and Young 2012). In addition to sepsis-associated encephalopathy, MV may remotely affect cerebral function due to brain-lung interactions and is associated with neurocognitive complications in a considerable portion of critically ill, mechanically ventilated patients (Slutsky and Tremblay 1998; Ely et al. 2004).

While the pathophysiology of neurocognitive deficits in critically ill patients is thought to be complex and multifactorial, the immune activation and systemic inflammation elicited by either the septic condition or the use of ventilatory support have been proposed to play a critical role in neuropsychological alterations (Chen et al. 2015; Turon et al. 2018; Sparrow et al. 2021). Systemic inflammation has a substantial impact on the central nervous system (CNS), as evidenced by the neuroinflammation pathologically occurring in the brain via an impaired blood–brain barrier. Numerous efforts have been made to clarify the mechanism underlies how neuroinflammation develops in response to systemic infection or mechanical ventilation and further contributes to resulting cerebral consequences (Hoogland et al. 2015; Giordano et al. 2021). For example, accumulating experimental evidence in rodents has suggested that systemic challenge caused by intraperitoneal injection of lipopolysaccharide (LPS) or MV is significantly associated with reactive microglia, the resident macrophage-like cells

within the brain for monitoring and sustaining the balance of the microenvironment within the CNS (Terrando et al. 2010; Chen et al. 2012, 2016). Microglia are crucial for the maintenance of synaptic integrity by synaptic remodelling and have also been implicated in pathological synapse loss and dysfunction following injury, inflammation, or nervous system degeneration (Werneburg et al. 2020; Cao et al. 2021). For example, microglial engulfment of neuronal synapses contributes to cognitive dysfunction, and synapse numbers are decreased in the dorsolateral prefrontal cortex of patients suffering mental illness, such as suppression (Kang et al. 2012). NADPH oxidase 2 (NOX2) enzymes critically contribute to reactive microglia through the generation of superoxide anions, such as reactive oxygen species (ROS), and subsequently lead to neuronal dysregulation such as synaptic plasticity impairment and neuronal death, which affects neurocognitive function (Qiu et al. 2016; Huang et al. 2020).

Many molecular targets have been proposed to address the mechanism of reactive microglia and the resulting neuronal dysfunction or damage, such as angiotensin II type 2 receptor (AGTR2). In addition to the cardiovascular and renal systems, abundant levels of AGTR2 within the CNS locally expressed on a variety of cell types, including microglia, astrocytes, and neurons of the prefrontal cortex, hippocampus, and basal ganglia, have been extensively studied in the context of neuroprotection and cognition (Lenkei et al. 1996; de Kloet et al. 2016; Jackson et al. 2018). Recently, using AGTR2-deficient mice or an orally effective AGTR2 agonist, compound 21 (C21), it has been reported that direct AGTR2 stimulation is neuroprotective and improves cognitive impairment in animal models with cerebral ischemia stroke (Alhusban et al. 2015; Schwengel et al. 2016; Eldahshan et al. 2019) and Alzheimer's disease (Jing et al. 2012; Royea et al. 2020). This neuroprotective action of AGTR2 has been thought to be related to a microglia-dependent mechanism. It has been demonstrated that AGTR2 stimulation using C21 lessens NADPH oxidase (NOX)-mediated reactive microglia and participates in the modulation of aberrant microglial polarization (Bhat et al. 2019; Jackson et al. 2020; Jackson-Cowan et al. 2021). It is largely unclear whether and how AGTR2 is involved in the development of cognitive deficits caused by a critical illness. Based on these findings, we hypothesized that AGTR2 activation might be a suitable strategy for mitigating cognitive deficits under critically ill conditions, and this beneficial effect was related to the reversal of reactive microglia and synaptic abnormalities.

To test this hypothesis, we utilized a clinically relevant mice model subjected to a single intraperitoneal injection of LPS followed 2 h later by MV (10 ml/kg, lasting for 2 h) to mimic, at least to some extent, the complex settings of ventilator-treated patients with preexisting sepsis in the present study (Ding et al. 2013, 2018; Zhang et al. 2021). Both the hippocampus and prefrontal cortex were selected

throughout the following study because areas commonly thought to be highly linked to neurocognitive processes are often reported brain regions of interest in the majority of studies when it has been mentioned that reactive microglia respond to systemic inflammation (Hoogland et al. 2015). By using a combination of pharmacological tools, behavioral testing paradigm, microglial structural reconstruction, and confocal imaging, we demonstrated here that the AGTR2 agonist C21 alleviates behavioral deficits in mice subjected to LPS/MV, via mechanisms that involve reactive microglia and abnormal synaptic plasticity in NOX2-derived ROS and the PKC-NF κ B pathway. Our findings provide experimental evidence to support the molecular and cellular basis for AGTR2 as a target candidate against cognitive deficits after exposure to critically ill conditions.

Methods

Animals

All animal protocols were approved by the Animal Use and Ethics Committee, Anhui Medical University. Male C57BL/6 J mice (purchased from Jackson Laboratory) and *Cx3cr1-GFP* mice, *Thy1-YFP* mice (kindly offered by Professor Zhi Zhang), aged 8–12 weeks, weighing approximately 25 g, were used in the experiments. Mice were housed in a specific pathogen-free environment with controlled ambient temperature ($22 \pm 25^\circ\text{C}$) and humidity ($50\% \pm 10\%$) under a 12 h light–dark cycle (lights on from 07:00 to 19:00) with water and food available ad libitum. The animals were acclimated to the housing conditions for 1 week before the experiments.

Animal Model

A two-hit model with LPS challenge followed by MV was used, as described previously (Ding et al. 2018; Zhang et al. 2021). Briefly, 2 h before receiving MV, mice were anesthetized using isoflurane and pretreated with an intraperitoneal injection of LPS (Sigma, L-2880, *Escherichia coli*, serotype O26: 1 mg/kg) to induce systemic inflammation. Afterward, mice were anesthetized with an intraperitoneal injection of pentobarbital (50 mg/kg) before endotracheal intubation. Mice were ventilated for 120 min with a tidal volume of 10 mL/kg, a respiratory rate of 70 breaths/min, and a 1:1 inspiratory:expiratory ratio with room air (FiO₂ of 0.21) and without positive end-expiratory pressure, using a volume-driven small animal ventilator (RWD407, RWD Life Science: Shenzhen, China). The body temperature of the animals was maintained at 36°C throughout the procedure using a heating pad. In this study, the control treatment was

defined as those mice receiving the same volume of saline injection 2 h before anesthesia and being allowed to breathe spontaneously.

Open Field Test

All behavioral procedures were carried out in a sound-isolated room. Tests were recorded by the same investigator blinded to the grouping of mice. The apparatus was made up of a white Plexiglas chamber (50 cm \times 50 cm \times 25 cm) made of gray polyvinyl chloride. The mice were gently placed in the center. A camera recorded the routes of the mice as they moved for a period of 6 min. Total distance travelled were calculated by EthoVision XT 14 software (Noldus, Wageningen, the Netherlands). The chamber was cleaned with 75% ethanol and clean water after each test to remove olfactory cues.

Fear Conditioning Test

On the training day, the animals were placed into an enclosed training chamber and allowed to explore for 180 s. Then, the mice were exposed to a tone (30 s, 70 dB, 3 kHz), followed by a 2 s foot shock (0.75 mA). Afterward, the mice were left in the chamber for an additional 30 s before being returned to their home cage. On the test day, the mice were re-exposed in the same chamber for 5 min for the contextual fear conditioning test. The animal was placed 2 h later into another test chamber for the cued fear conditioning test, which had a different context and smells from the first test chamber in relative lightroom. After a 3 min exploratory period, the tone was then turned on for 3 cycles, each cycle for 30 s followed by a 1-min intercycle interval (4.5 min in total). The chamber was thoroughly cleaned with 75% ethanol after each trial. Animal behavior in these two chambers was video recorded. The length of freezing behavior in 5 min in the first chamber (context-related) and 4.5 min in the second chamber (tone-related) was recorded by an observer who was blinded to the group assignment. Freezing was defined as a completely immobile posture except for respiration.

Treatment Grouping

To determine the optimal dose of C21 against the reactive microglia, C21 at 0.03, 0.3, or 3 mg/kg dissolved in saline solution was injected intraperitoneally once daily for seven consecutive days before the two-hit model. Animals in the control groups received the same volume of vehicle (normal saline) at the corresponding time points.

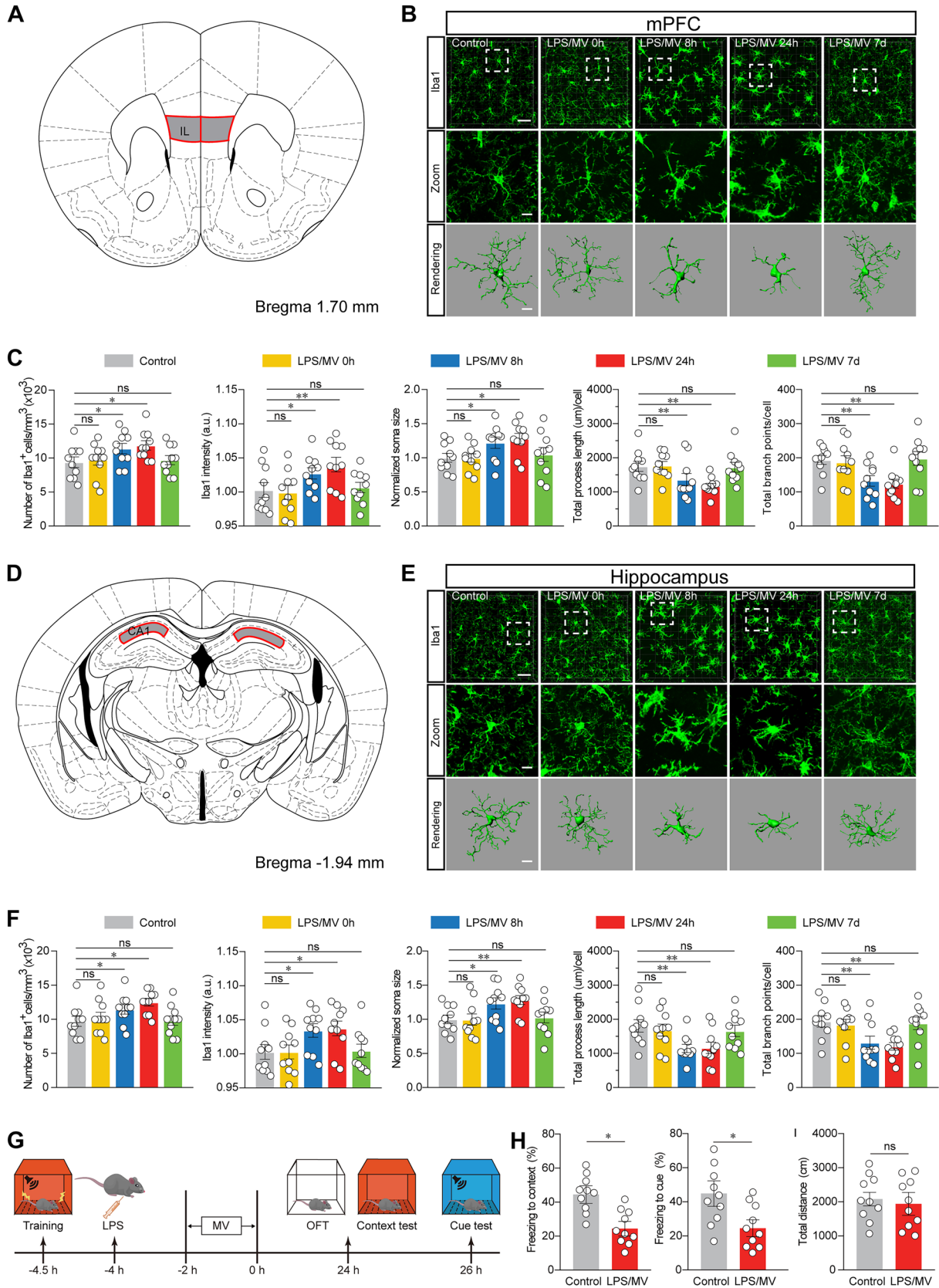


Fig. 1 Microglial activation develops in response to LPS/MV cotreatment. **A** Representations from Paxinos & Franklin mouse atlas of regions of interest analysed. IL region of mPFC. **B** Representative images from LPS/MV-treated mice at different time points. Iba1 immunostaining and three-dimensional (3D) reconstruction of microglia in the mPFC was shown. Scale bars, 40 μm (overview) and 10 μm (Zoom and Rendering). **C** Quantification of Iba1⁺ number and intensity, soma size, Imaris-based semi-automatic quantification of Iba1⁺ microglia morphometry in the mPFC. **D** Representations from Paxinos & Franklin mouse atlas of regions of interest analysed. CA1 region of the dorsal hippocampus. **E** Representative images from LPS/MV-treated mice at different time points. Iba1 immunostaining and three-dimensional (3D) reconstruction of microglia in the hippocampus was shown. Scale bars, 40 μm (overview) and 10 μm (Zoom and Rendering). **F** Quantification of Iba1⁺ number and intensity, soma size, Imaris-based semi-automatic quantification of Iba1⁺ microglia morphometry in the hippocampus. **G** Schematic timeline of behavioral tests. **H** The analysis results of FCT in control and LPS/MV-treated mice. **I** The analysis results of OFT in control and LPS/MV-treated mice. All data were presented as mean \pm SEM. * $p < 0.05$; ** $p < 0.01$; *** $p < 0.001$; ns, not significant. For detailed statistics information, see Table S1. Abbreviations: mPFC, medial prefrontal cortex; LPS, lipopolysaccharide; MV, mechanical ventilation; OFT, Open Field Test; FCT, Fear Conditioning Test

Immunofluorescent Staining

Mice were deeply anesthetized with an intraperitoneal injection of pentobarbital (50 mg/kg) and perfused intracardially with saline and 4% (w/v) paraformaldehyde. The brain was removed and postfixed in 4% (w/v) paraformaldehyde overnight, before being placed in 30% (w/v) sucrose overnight for dehydration. Coronal frozen Sects. (40 μm thick) were cut by cryostat (Leica CM1860, Germany) for further immunoreactivity staining. The sections were blocked in 5% (w/v) bovine serum and 0.5% (v/v) Triton X-100 for 1 h at room temperature. Following blocking, the sections were incubated with primary antibodies diluted with blocking solution, including anti-ionized calcium-binding adapter molecule 1 (Iba1) (1:500, rabbit, Wako and 1:500, goat, Abcam), anti-MHCII (1:500, mouse, Abcam), anti-CD68 (1:500, mouse, Abcam) and anti-PSD95 (1:500, Goat, Abcam) and anti-synaptophysin (1:100, rabbit, Cell signaling), anti-GFAP (1:200, mouse, Cell signaling), anti-NeuN (1:500, mouse, Abcam), and anti-NOX2 (1:500, mouse, Santa Cruz), at 4 $^{\circ}\text{C}$ overnight. Next, the sections were incubated with corresponding fluorophore-conjugated secondary antibodies diluted with blocking solution for 1.5 h at room temperature, followed by staining with 4,6-diamidino-2-phenylindole (DAPI; 1:2000, Sigma) for 3 min. Finally, coverslips were mounted after adding antifade mounting media (VECTASHIELD Vibrance), and fluorescence signals were visualized using a Leica DM2500 camera and a Zeiss LSM880 microscope. Further analyses, such as analysis of fluorescence intensity and colocalization, were conducted using ImageJ software (Fiji edition, NIH). All the experimental details are described elsewhere (Pan et al. 2022).

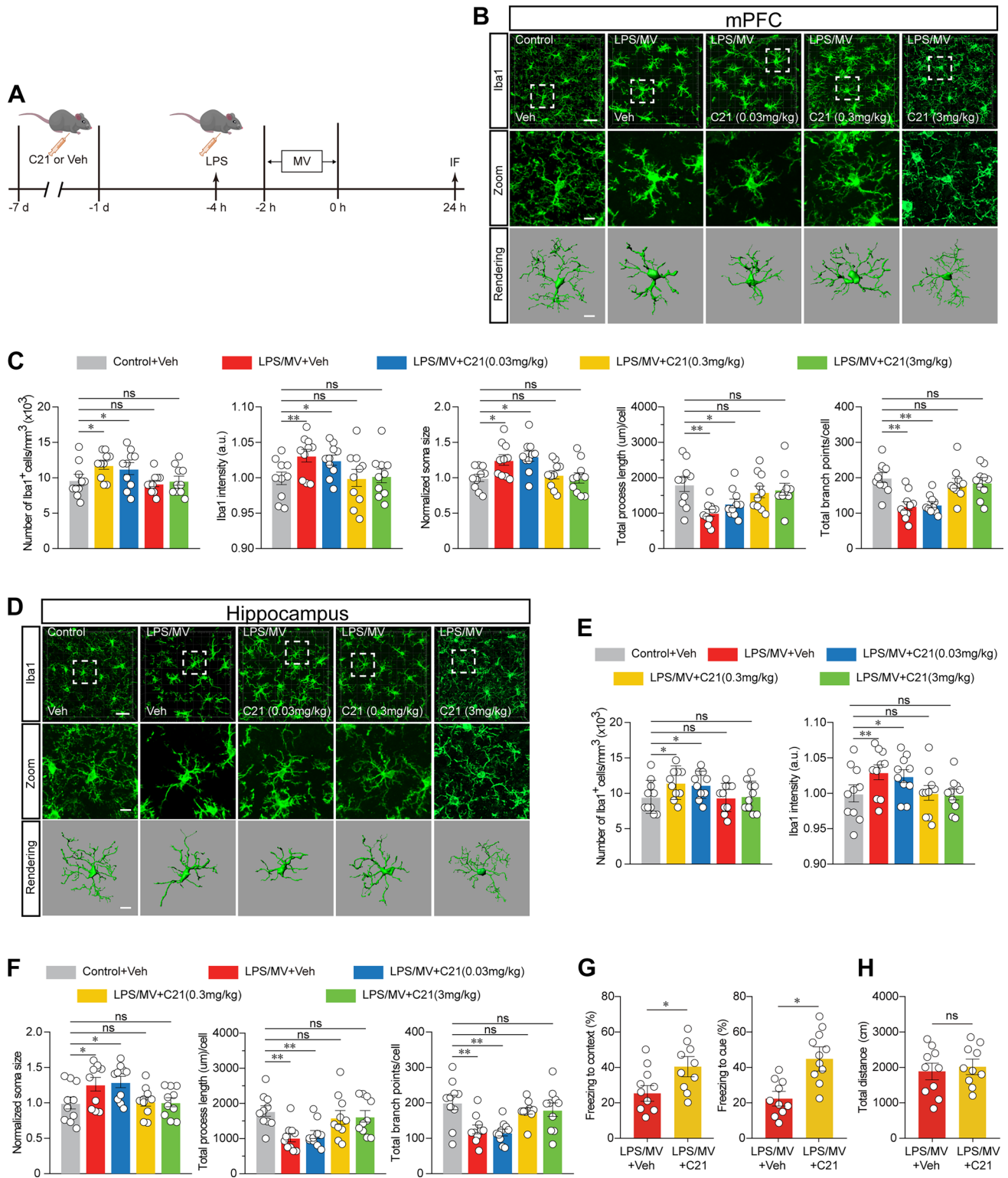
Morphological Analysis

For morphometric analysis, as mentioned previously (Pan et al. 2022), confocal images of Iba1-positive cells were visualized and acquired by a confocal laser-scanning microscope (Carl Zeiss LSM880, Germany) with a 40 \times objective at 30- μm intervals along the z-axis. We opened the confocal Z-stacks image file and selected “Add New Filaments | Create | Calculate Diameter of Filaments from Image”. The diameter should be between 0.25 μm and 15 μm . We modulated the “Starting Point” and “Seed Point Thresholds” of dendrites according to the actual size and selected “Remove Seed Points Around Starting Points” and set the diameter of “Sphere Regions” as 30 μm . The number of balls was the number of myeloid cells in the image counted per mm³ according to the volume of the image. We adjusted the threshold of the dendrites. In the spine “Points Diameter” step, we deselected the “Detect Spines” option. Finally, we clicked “statistics | Detailed | Specific Values | dendrite length” and saved the data as a.xls file. The data were used as a measure of myeloid cell morphology, such as the number of endpoints and process length. Two images were randomly picked from each mouse, and the mean result was used for morphological analysis. Three-dimensional reconstruction of myeloid cells was performed using IMARIS software.

Microglial engulfment was analyzed using IMARIS software to create a 3D surface rendering of the microglia, with a threshold established to ensure accurate reconstruction of microglial processes, which was then used for subsequent reconstructions. PSD95⁺ and synaptophysin⁺ puncta were reconstructed using the IMARIS “Spots” function. We used the IMARIS MATLAB-based (MathWorks) plugin “Split into Surface Objects” to assess the number of PSD95⁺ and synaptophysin⁺ puncta entirely within the microglial surface. Two images randomly picked from each mouse were reconstructed, each having at least ten cells, for six mice in each group. The mean result was used for morphological analysis. All the experimental details were described previously (Cao et al. 2021).

To assess dendritic spine elimination, images were acquired from *Thy1-YFP* mice and dendritic spines were randomly selected by an observer blinded to the experimental purpose. The selected spines were then assessed to ensure that they were resolved on the images. In detail, approximately 30 dendrites from three mice in each group were analyzed using the plugin NeuronJ 1.4.3 in ImageJ software (Fiji edition, NIH). Thereafter, the plugin Cell Counter was used to calculate the number of spines on these dendrites. All the experimental details were described previously (Cao et al. 2021).

For analysis of microglial processes and neuronal dendrite contacts, imaging was performed on a Zeiss LSM880 microscope using a 100 \times /1.4 NA oil objective, and imaging



parameters (laser power, gain and offset) were consistent across all experiments. Both Iba1⁺ microglia and YFP⁺ dendrites were accurately reconstructed using the “Surface” function in IMARIS, and initially-established thresholds were then used for subsequent reconstructions. The

MATLAB-based IMARIS plugin “Surface-Surface Contact Area,” was used to measure the size of contact areas between microglial processes and neuronal dendrites. All the experimental details were described previously (Cao et al. 2021).

Fig. 2 AGTR2 agonist rescues microglia activation and memory decline. **A** Schematic timeline of experiment. Control and LPS/MV-stimulated mice were pre-treated with vehicle, and LPS/MV-stimulated mice pre-treated with different concentrations of C21 were designated as LPS/MV+C21 (0.03, 0.3, and 3 mg/kg) groups. **B** The results of Iba1 immunostaining and 3D reconstruction of microglia in the mPFC was shown. Scale bars, 40 μ m (overview) and 10 μ m (Zoom and Rendering). **C** Quantification of Iba1⁺ number, intensity, soma size, and Iba1⁺ microglia morphometry was measured by Imaris-based semi-automatic quantification in the mPFC. **D** The results of Iba1 immunostaining and 3D reconstruction of microglia in the hippocampus was shown. Scale bars, 40 μ m (overview) and 10 μ m (Zoom and Rendering). **E** Quantification of Iba1⁺ number and intensity in the hippocampus. **F** Quantification of Iba1⁺ soma size, and Imaris-based semi-automatic quantification of Iba1⁺ microglia morphometry in the hippocampus. **G** The results of FCT was analysed in Veh and C21-treated mice. **H** The results of OFT was analysed in Veh and C21-treated mice. All data were presented as mean \pm SEM. * $p < 0.05$; ** $p < 0.01$; *** $p < 0.001$; ns, not significant. For detailed statistics information, see Table S1. Abbreviations: AGTR2, angiotensin type 2 receptor; Veh, vehicle; C21, compound 21

Fluorescence-activated Cell Sorting

Mice were anesthetized with an intraperitoneal injection of pentobarbital (50 mg/kg). Subsequently, mice were perfused intracardially with 20 ml of 0.1 M cold Hanks' balanced salt solution (HBSS), followed by a rapid collection of hippocampus and prefrontal cortex tissues (10 pooled animals per N), which were washed with cold HBSS and chopped into small pieces on ice. Small tissue was mechanically homogenized using a 23G needle to produce single-cell suspensions, which were filtered through a 70 μ m cell strainer. After 70%-30% Percoll gradient (Sigma, US) separation, the single-cell suspension was isolated from the interface and filtered with a 200 μ m nylon mesh prior to staining with antibody staining. Microglia were labelled with CD11b-PC5.5 (1:200, Biolegend), and sorted by BD FACSAria III (BD, USA) for subsequent qPCR experiments.

Real-time PCR

Total RNA was extracted from isolated microglia using TRIzol reagent (Vazyme, Nanjing, China) and quantified using NanoVue plus (GE, US). Approximately 500 ng of total RNA was reverse transcribed using StarScript II First-strand cDNA Synthesis Mix with gDNA Remover (GenStar, Beijing, China) in 20 μ l reactions following the manufacturer's protocol. Quantitative real-time PCR (qPCR) for IL-1 β , TNF- α , BDNF, and NOX2 was performed on an Applied Biosystems StepOne™ Real-Time PCR System using the 2 \times TSINGKE Master qPCR Mix (SYBR Green I) (Tsingke Biotechnology, Beijing, China). Gene-specific primers were purchased from Tsingke Biotechnology. The primer sequences were as follows:

IL-1 β (forward 5'-TTCAGGCAGGCAGTATCACTC-3', reverse 5'-GAAGGTCCACGGGAAAGACAC-3')
 TNF- α (forward 5'-CCTGTAGCCCACGTCGTAG-3', reverse 5'-GGGAGTAGACAAGGTACAACCC-3')
 BDNF (forward 5'-GCCTTTGGAGCCTCCTCC TCTAC-3', reverse 5'-GCGGCATCCAGGTAATTTT-3')
 NOX2 (forward 5'-GGGAAGTGGGCTGTGAATGA-3', reverse 5'-CAGTGCTGACCCAAGGAGTT-3')

In situ ROS Assay

Detection of ROS production in vivo in mice was conducted by using dihydroethidium (DHE, Beyotime, China) as previously described (Zhang et al. 2019; Liu et al. 2020). Briefly, mice were injected with DHE (0.01 mg/g body weight, intraperitoneal injection) 4 h before sacrifice. Oxidized DHE (ox-DHE) emits bright red fluorescence, which can be detected at an emission wavelength of 570 nm. The fluorescent signal was captured with a Zeiss LSM880 microscope, and the threshold-based area of DHE-positive staining was quantified using the ImageJ system.

Western Blotting

Mice were deeply anesthetized and subsequently intracardially perfused with 20 ml of 0.1 M cold PBS. The hippocampus and prefrontal cortex were collected and washed twice with ice-cold PBS and lysed in ice-cold RIPA lysis buffer containing 1 mM PMSF. The supernatant was obtained by centrifuging at 12,000 g at 4 °C for 15 min. The protein concentration was detected with Pierce™ BCA protein assay kit (Thermo, USA). Twenty micrograms of protein per lane was loaded on a 10% SDS-polyacrylamide gel and subsequently transferred to a nitrocellulose membrane, rinsed in TRIS buffered saline (TBS), and blocked in 5% nonfat milk in TBS with 0.1% Tween (TBS-T) for 1 h at room temperature. After rinsing in TBS-T, membranes were incubated 4 °C overnight in primary antibodies against β -Actin (1:500, Absin Bioscience, China), anti-IL-1 β (1:500, Absin Bioscience, China), anti-TNF- α (1:500, Absin Bioscience, China), anti-BDNF (1:500, AbCam, UK), anti-phospho-NCF1 (1:500, Bioss, China), anti-phospho-PP2A (1:500, Bioss, China), anti-phospho-PKC δ (1:500, Bioss, China), anti-p65 (1:1000, CST, US), anti-phospho-p65 (1:1000, CST, US), anti-I- κ B (1:500, Affinity, US), and anti-phospho-I- κ B (1:500, Affinity, US). Blots were washed in TBS-T and incubated for 1 h in peroxidase-labelled secondary antibody (1:5000, Thermo Scientific) at room temperature. Protein bands were visualized by chemiluminescence reagent (Biosharp, China) and quantified using ImageJ software.

Statistical Analysis

GraphPad Prism 8 (GraphPad Software, Inc., US) was used for statistical analysis and graphing. The QQ-plots were used

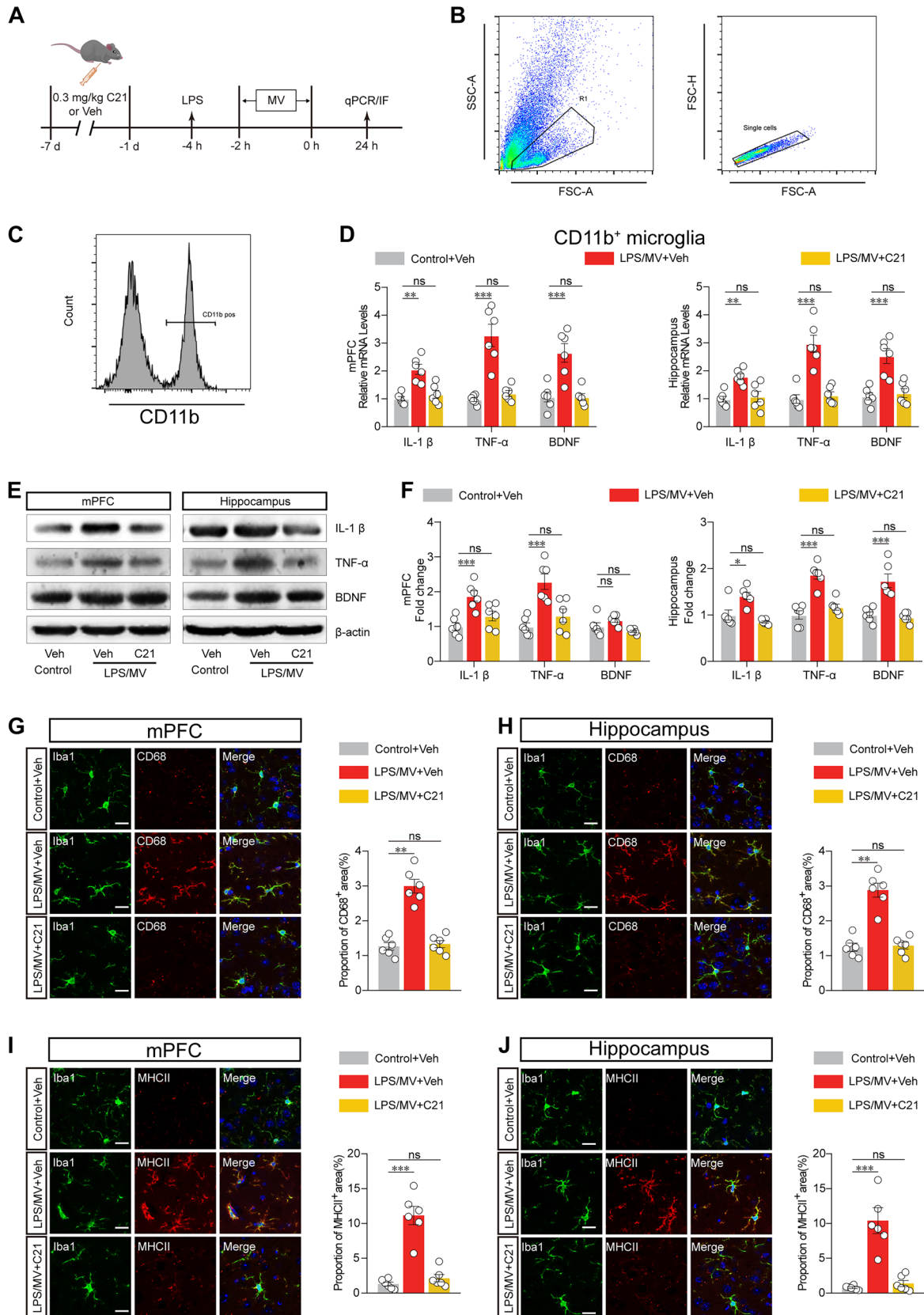


Fig. 3 AGTR2 agonist reduces microglial functional markers and inflammatory factors. **A** Schematic timeline, and mice were randomly divided into three groups as control + Veh, LPS/MV + Veh, and LPS/MV + C21. **B-C** Workflow diagram and the scheme of flow cytometry and cell sorting. **D** The gene mRNA expression of IL-1 β , TNF α , and BDNF in CD11b-labelled microglia from the mPFC (left panel) and hippocampus (right panel). **E** Western blot analysis of IL-1 β , TNF α , and BDNF protein levels in the mPFC (left panel) and hippocampus (right panel). **F** Semi-quantification for different proteins expression were normalized in the mPFC (left panel) and hippocampus (right panel). **G** Representative images (left panel) and analysis results (right panel) of CD68 in Iba1⁺ cell from the areas of mPFC. Scale bar, 20 μ m. **H** Representative images (left panel) and analysis results (right panel) of CD68 in Iba1⁺ cell from the areas of hippocampus. Scale bar, 20 μ m. **I** Representative images (left panel) and quantitative analysis (right panel) of MHCII in the areas of mPFC. Scale bar, 20 μ m. **J** Representative images (left panel) and quantitative analysis (right panel) of MHCII in the areas of hippocampus. Scale bar, 20 μ m. All data were presented as mean \pm SEM. * $p < 0.05$; ** $p < 0.01$; *** $p < 0.001$; ns, not significant. For detailed statistics information, see Table S1

to verify the assumptions before the t-test, ANOVA, and descriptive statistics. We conducted statistical comparisons between two groups using Student's *t*-tests. ANOVA and Bonferroni post hoc analysis were used in analyses with multiple experimental groups. All data are expressed as the mean \pm SEM and significance levels are indicated as * $p < 0.05$, ** $p < 0.01$ and *** $p < 0.001$. P values are not provided as exact values when they are less than 0.0001.

Results

Microglial Activation Develops in Response to Cotreatment with LPS/MV

Given that the hippocampus and prefrontal cortex are the two most vulnerable areas in neurocognitive dysfunction, we selected those two areas throughout the following study. To determine whether microglia were activated in response to cotreatment with LPS/MV, we performed morphological reconstruction of microglia at consecutive time points by using Iba1-staining and further assessed the temporal changes in processes in branch endpoints and length, which is known to correlate well with reactive microglial status (Cao et al. 2021; Pan et al. 2022). Experimental studies previously have shown that microglia were moderately active within hours after a single challenge with LPS, reaching their profound activation state after 8 h to 2 days and subsequently returning to their normal surveilling state after 7 days (Hoogland et al. 2015). In line with the published results, our findings revealed that a significant status of reactive microglia, which was manifested by the shorter processes and decreased branch points, substantially occurred 24 h after a cotreatment of LPS/MV (Fig. 1A-F).

Locomotor activity and behavioural phenotypes were evaluated 24 h after the co-treatment of LPS/MV (Fig. 1G). In the FCT, the cotreatment of LPS/MV significantly decreased the percentage of freezing time compared with the control group (Fig. 1H). In the OFT, there was no significant difference in the total distance or time/distance spent in the center area between the control-treated group and the LPS/MV-treated group (Fig. 1I). These data have shown that the mice subjected to LPS/MV display memory impairments, without any changes in locomotor activity.

AGTR2 Agonist Rescues Microglia Activation and Memory Decline

Given that the neuroprotective role of AGTR2 is thought to be related to its suppressive action on microglia-mediated neuroinflammation, we utilized the AGTR2 pharmacological agonist C21 at different dosages (0.03, 0.3, and 3 mg/kg) to observe the resulting impacts on the reactive microglia (Fig. 2A). Compared with the vehicle-control, pretreatment of C21 with 7 continuous days at 0.3 and 3 mg/kg, but without 0.03 mg/kg, significantly altered the microglial structural traits both in the hippocampus and prefrontal cortex in mice subjected to LPS/MV (Fig. 2BF). Our findings showed that C21 restrained the microglia in a dose-dependent manner, and a dose of 0.3 mg/kg was chosen for the following experiments. For further validation, we subsequently sought to determine the impact of the AGTR2 agonist C21 on behavioural deficits induced by cotreatment with LPS/MV. Compared with the vehicle-control, the FCT results indicated that AGTR2 stimulation rescued memory impairments in C21-treated mice following cotreatment with LPS/MV (Fig. 2G), but without any alterations in locomotor activity according to OFT results (Fig. 2H).

In addition to the alterations of morphological traits, activated microglia are highly characterized by producing high levels of proinflammatory cytokines (such as IL-1 β and TNF- α) and brain-derived neurotrophic factor (BDNF) (Fig. 3A). We thus isolated the CD11b-labelled microglia using FACS from the hippocampus and prefrontal cortex tissues, and further quantified the mRNA levels of IL-1 β , TNF- α , and BDNF using qPCR (Fig. 3B, C). As shown in Fig. 3D, an increase in IL-1 β , TNF- α , and BDNF levels in response to LPS/MV was observed in isolated microglia, which was prevented by pretreatment with C21. Western blot analysis of these protein levels also showed the same results (Fig. 3E, F). Furthermore, CD68 and MHCII markers, which are associated with reactive microglia status, were also found to be increased in mice subjected to cotreatment with LPS/MV. In line with the findings that C21-elicited suppression of microglial morphological phenotypes, pretreatment with C21 significantly reduced the enhancement of CD68 and MHCII levels in those LPS/MV-treated mice (Fig. 3G-J).

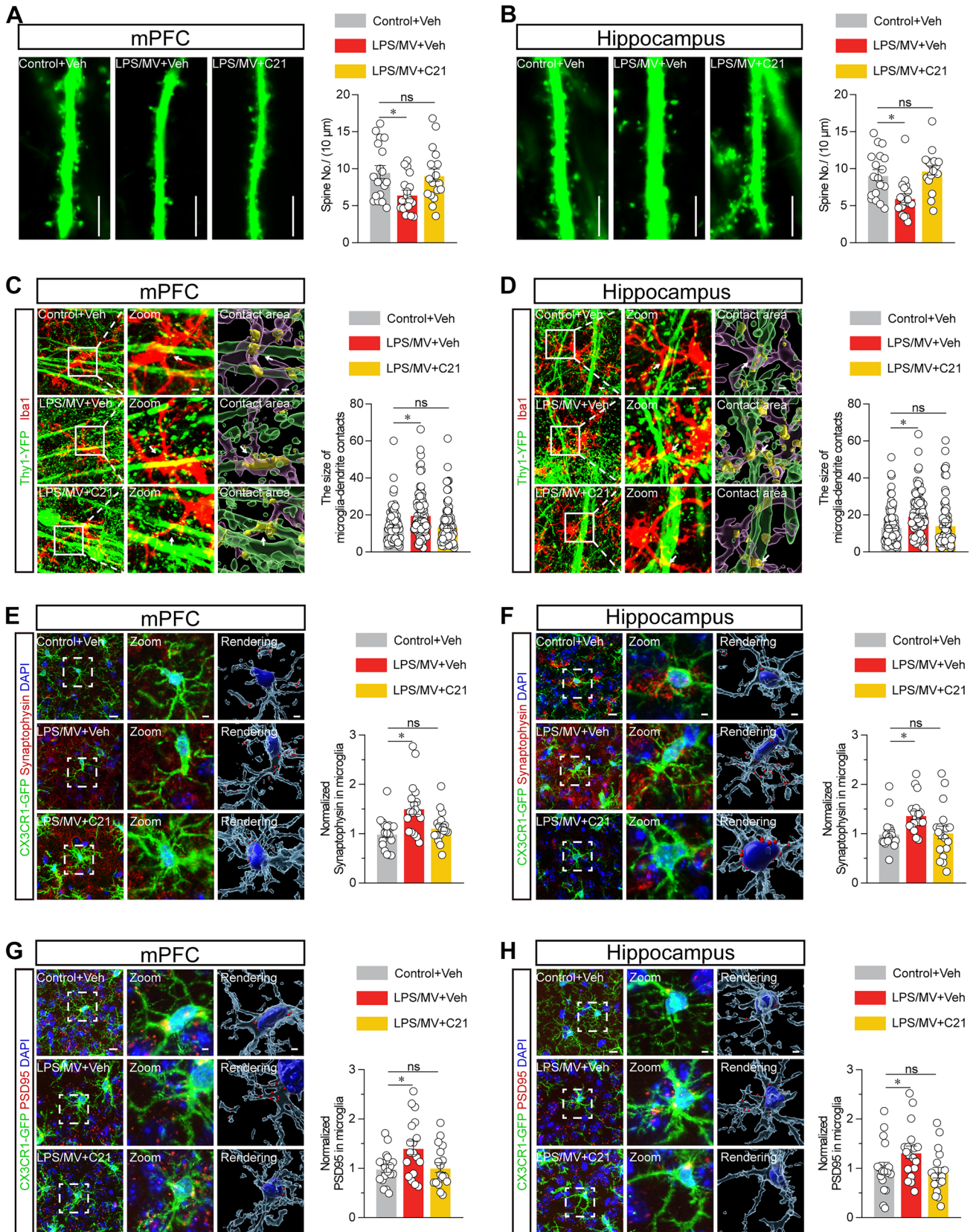


Fig. 4 AGTR2 agonist reduces microglial engulfment of neuronal spines and phagocytosis of synapses. **A** Representative images of neuronal dendrites (left panel) and summarized data for spine numbers per 10 μm (right panel) were displayed in the mPFC from *Thy1-YFP* mice. Scale bar, 10 μm . **B** Representative images of neuronal dendrites (left panel) and summarized data for spine numbers per 10 μm (right panel) were displayed in the hippocampus from *Thy1-YFP* mice. Scale bar, 10 μm . **C** Reconstructed images of Iba1⁺ microglia (red) and YFP⁺ neuronal dendrites (*Thy1-YFP* mice) (left panel), and summarized data for the size of microglia-dendrite contacts (right panel) in the mPFC. Scale bars, 5 μm (overview) and 2 μm (inset). **D** Reconstructed images of Iba1⁺ microglia (red) and YFP⁺ neuronal dendrites (*Thy1-YFP* mice) (left panel), and summarized data for the size of microglia-dendrite contacts (right panel) in the hippocampus. Scale bars, 5 μm (overview) and 2 μm (inset). **E** Representative images and 3D surface rendering of Iba1⁺ microglia containing synaptophysin puncta (left panel), and quantification of synaptophysin puncta in microglia (right panel) in the mPFC as indicated. Scale bars, 10 μm (overview) and 2 μm (inset and rendering). **F** Representative images and 3D surface rendering of Iba1⁺ microglia containing synaptophysin puncta (left panel), and quantification of synaptophysin puncta in microglia (right panel) in the hippocampus as indicated. Scale bars, 10 μm (overview) and 2 μm (inset and rendering). **G** Representative images and 3D surface rendering of Iba1⁺ microglia containing PSD95⁺ puncta (left panel), and quantification of PSD95⁺ puncta in microglia (right panel) in the mPFC as indicated. Scale bars, 10 μm (overview) and 2 μm (inset and rendering). **H** Representative images and 3D surface rendering of Iba1⁺ microglia containing PSD95⁺ puncta (left panel), and quantification of PSD95⁺ puncta in microglia (right panel) in the hippocampus as indicated. Scale bars, 10 μm (overview) and 2 μm (inset and rendering). All data were presented as mean \pm SEM. * $p < 0.05$, ** $p < 0.01$, and *** $p < 0.001$; ns, not significant. For detailed statistics information, see Table S1

AGTR2 Agonist Reduces Microglial Engulfment of Neuronal Spines

Microglia are important phagocytic cells that participate in synapse remodelling by conducting synaptic pruning, and disrupted synaptic pruning is associated with concomitant reactive microglia in neurological disease (Tonnie and Trushina 2017; Copley et al. 2018). We observed synaptic dysfunction in response to a cochallenge with LPS/MV, which was morphologically manifested by a reduction in the number of synaptic spines in LPS/MV-treated *Thy1-YFP* mice (Fig. 4A, B). We next examined the interactions of microglial processes and neuronal dendritic spines in the hippocampus and prefrontal cortex. First, we investigated the microglia-dendrite contact using Iba1-staining to reconstruct the morphology of microglial processes in *Thy1-YFP* mice, which can be visualized with dendritic spines of neurons expressing YFP. The contact of microglial processes (red) and neuronal dendrites (green) is shown in Fig. 4C, D and the size of microglia-dendrite contact areas was abundantly elevated in LPS/MV-treated mice, which was significantly reduced by pretreatment with C21 (Fig. 4C, D). In addition to microglia-dendrite contact, three-dimensional reconstruction further revealed that abundant immunoreactive puncta (red) of synaptic protein markers, such as postsynaptic

marker PSD95 or presynaptic marker synaptophysin, and Cx3cr1-labelled microglial processes (green) colocalized in *Cx3cr1-GFP* mice following a co-treatment of LPS/MV, but not control-treated mice (Fig. 4E-H). Compared with the vehicle control, these synaptic alterations were significantly reduced by pretreatment with C21 (Fig. 4E-H). These results collectively showed that LPS/MV led to an increase in synaptic loss due to microglial phagocytosis and that these phenotypes were reversed upon intraperitoneal injection of preadministered C21.

AGTR2 Agonist Declines NOX2-derived ROS and PKC δ -NF κ B in Microglia

To elucidate how the AT₂R agonist C21 rescues the aberrant reactive microglia and dysregulated synaptic pruning, we further determined whether C21 produced any impacts on the high level of superoxides, such as ROS, which are thought to initiate or facilitate the downstream reactive microglia and neuronal dysfunction (Qiu et al. 2016; Huang et al. 2020). Given that ROS production can be mediated through upregulation of NOX2, our data supported the idea that NOX2 is highly expressed in microglia from the hippocampus and prefrontal cortex, which may underpin the increased ROS generation observed following LPS/MV treatment (Fig. 5A, B). For further validation, we determined the change in mRNA levels of NOX2 from isolated microglia in control-treated and LPV/MV-treated mice. We observed that NOX2 mRNA was significantly enriched in response to LPS/MV in isolated microglia (Fig. 5C), and the same results were found at the protein level (Fig. 5D). Our findings indicated that NOX2, which is mainly detectable in Iba1-labelled microglia, in LPS/MV-treated mice was significantly higher than that in control-treated mice, and was subsequently lessened by pretreatment with C21 (Fig. 5E, F). We further identified ROS production by tracking the signals of oxidized dihydroethidine (ox-DHE), a marker for intracellular superoxide, and we found that ox-DHE staining was increased in response to LPS/MV, which was consistent with the increase in microglial NOX2 (Fig. 5G, H). Compared with the vehicle-control, pretreatment with C21 lessened ox-DHE staining in C21-treated mice following exposure to LPS/MV.

On the other hand, given that relevant signaling molecules, such as PKC, MAPKs, and NF- κ B, have been tightly linked to LPS-elicited reactive microglia and accompanying NOX2-induced ROS generation (Wen et al. 2011), we included NF- κ B, to explore whether it was involved in AT₂R-elicited beneficial actions and to identify whether AT₂R activation prevented p65 NF- κ B phosphorylation. In the present study, a substantial decrease in the ratio of total-p65/phosphorylated-p65 is attributed to higher levels of the phosphorylated p65 subunit, which indicates the activation

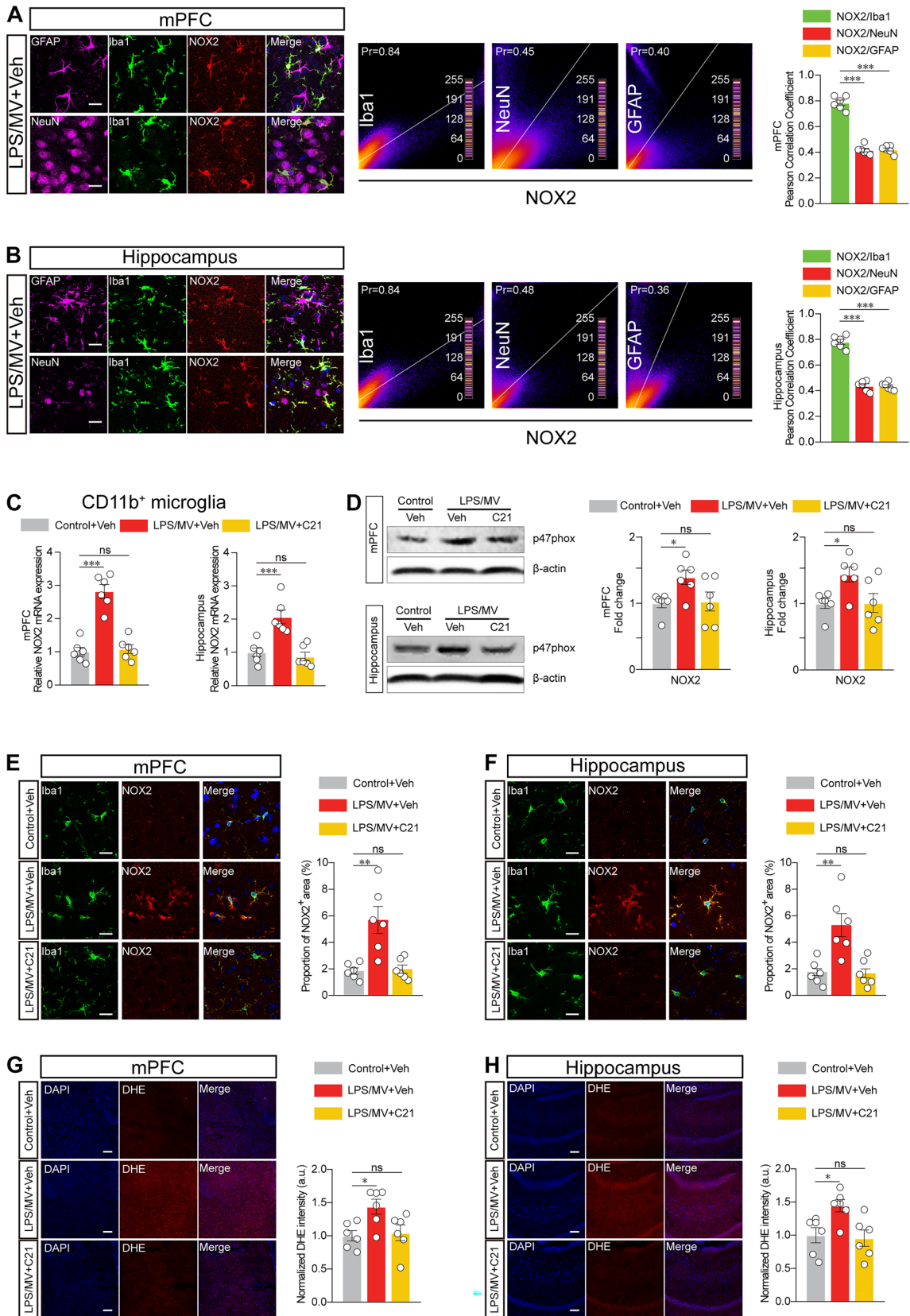


Fig. 5 AGTR2 agonist inhibits NOX2-derived ROS production in microglia. **A** Representative staining in the mPFC from LPS/MV-treated mice was shown. GFAP (violet), NeuN (violet), Iba1 (green), NOX2 (red), and DAPI (blue), and the co-localization of NOX2/Iba1, NOX2/NeuN, or NOX2/GFAP was analyzed by The Pearson's Correlation Coefficient test in the mPFC. Scale bar, 20 μ m. **B** Representative staining in the hippocampus from LPS/MV-treated mice was shown. GFAP (violet), NeuN (violet), Iba1 (green), NOX2 (red), and DAPI (blue), and the co-localization of NOX2/Iba1, NOX2/NeuN, or NOX2/GFAP was analyzed by The Pearson's Correlation Coefficient test in the hippocampus. Scale bar, 20 μ m. **C** Gene expression of NOX2 from CD11b-labelled microglia in the areas of mPFC (left) and hippocampus (right). **D** Western blot analysis of NOX2 protein levels (left), and Semi-quantification for proteins expression were normalized (right) in the mPFC and hippocampus. **E** Representative images (left) and the analysis (right) of NOX2 in the Iba1⁺ cell of mPFC. Scale bar, 20 μ m. **F** Representative images (left) and the analysis (right) of NOX2 in the Iba1⁺ cell of hippocampus. Scale bar, 20 μ m. **G** Representative images (left) and quantitative analysis (right) of immunostaining for DHE in the mPFC. Scale bar, 100 μ m. **H** Representative images and quantitative analysis of immunostaining for DHE in the hippocampus. Scale bar, 100 μ m. All data were presented as mean \pm SEM. * $p < 0.05$, ** $p < 0.01$, and *** $p < 0.001$; ns, not significant. For detailed statistics information, see Table S1. Abbreviations: NOX2, NADPH oxidase 2; DHE, dihydroethidine

of the NF- κ B signaling pathway after a C21 pretreatment (Fig. 6A-D). As an upstream signaling molecule, PKC δ is likely to be the major player that orchestrates microglial function in response to LPS insults by initiating NF- κ B-mediated transcriptional activation. It has been reported that the functional knockdown of PKC- δ attenuated ERK1/2 and p38 MAPKs phosphorylation, which subsequently led to the blockade of NF- κ B activation and iNOS overproduction in microglial cells. Findings from other works have demonstrated that AT2R induces the activation of PP2A, a protein phosphatase that leads to the dephosphorylation and inactivation of PKC in microglia (Bhat et al. 2019, 2021). In the present study, our results indicated that C21 phosphorylated PP2A and reduced phosphorylated PKC- δ (Fig. 6A-D). Our data supported the idea that stimulation of AT2R signaling by C21 prevented microglial activation through NOX2-induced ROS generation and PP2A-mediated inhibition of PKC and NF- κ B.

Discussion

The objectives of the current study were to determine whether pretreatment with C21 lessened cognitive deficits and weakened reactive microglia in mice subjected to LPS/MV, and to elucidate the possible underlying mechanism. Although AGTR2 exerts a beneficial role in improving cognitive function in multiple models of neurological diseases, this is the first study to demonstrate the potential role of the AGTR2 agonist C21 on concomitant neurocognitive

disorder in a mice model with high relevance to the critical care field. Given that a compelling relationship is implicated between systemic inflammation and reactive microglia in mediating acute brain dysfunction, we evaluated the impacts of C21 on reactive microglia and functional alterations in response to LPS/MV. Our findings indicated that pretreatment with C21 reduced reactive microglia, accompanied by suppression of microglia-mediated engulfment of neuronal synapses, in mice subjected to LPS/MV. In terms of the underlying mechanism, the C21-elicited ameliorative effect on reactive microglia and functions may be related to the NOX2-derived ROS PKC δ -NF κ B pathway.

The pathophysiological mechanisms of acute brain dysfunction in critically ill patients are poorly understood, but one of the main triggers that have been proposed is inflammation, which is commonly elicited by systemic infection, traumatic injury, surgical operation, and mechanical ventilatory support (Mei et al. 2021; Saito et al. 2021; Manabe and Heneka 2022). Inflammatory signals can be transmitted to brain by direct or indirect pathways and remotely affect the brain function as a consequence. Microglial cells, which are characterized by a very low threshold of activation, rapidly respond to noxious signals and exhibit highly functional plasticity in response to environmental alterations. In the present study, following the "two-hit" challenge of LPS plus MV, shorter processes and decreased branch points were found in the microglia of the mice subjected to LPS/MV. In addition to morphological changes, dramatic increases in MHCII, and CD68 markers, and the loss of synaptic protein markers were detected in microglia from PLS/MV-treated mice. Once surveilling microglia transform into reactive states in response to stress challenges, reactive microglia are implicated in the resulting neurocognitive outcome through a process known as microglia-dependent synaptic remodeling. This causal relationship has been evidenced by the fact that systemic inflammation-induced reactive microglia are accompanied by deficits in synaptic refinement, neuronal connectivity, and the proper extent of synaptic pruning (Wang et al. 2020; Cao et al. 2021). For example, Cao et al. found that early-life inflammation encodes long-lasting maladaptation of neurons to stress through excessive microglial engulfment of neuronal spines, resulting in the development of depression-like symptoms during adolescence (Cao et al. 2021).

Microglia have been found to be highly active in constantly responding to any type of brain homeostatic disturbance and are rapidly transformed from a highly ramified process to an amoeboid morphology under pathological conditions (Furube et al. 2018). In addition to morphological alterations, it has been convincingly shown that the proliferation of microglia is a concomitant event that is associated with disease pathological conditions, coinciding with the activation of microglia (Furube et al. 2018). In the mouse and human brain, microglial density

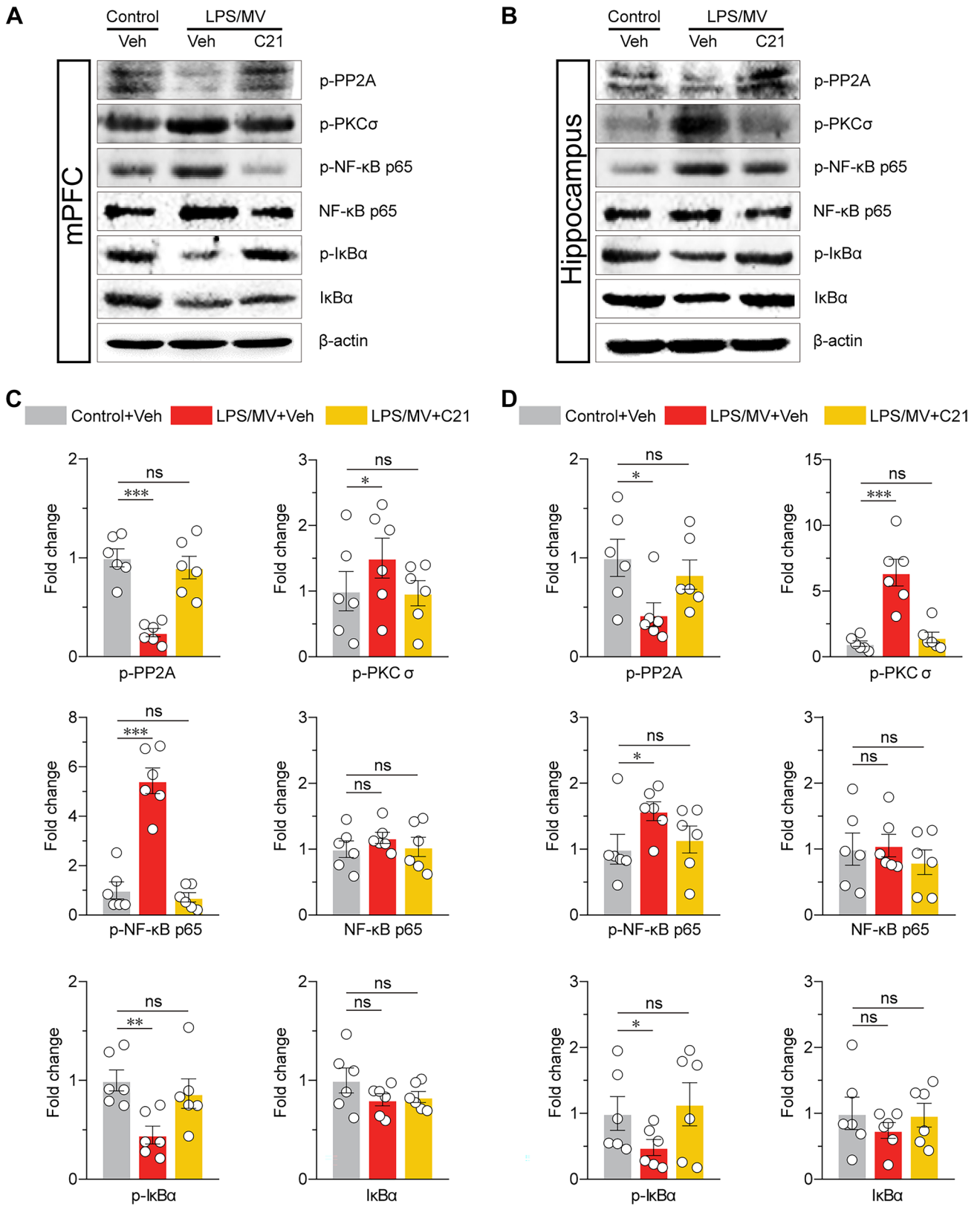


Fig. 6 AGTR2 agonist inhibits PKC δ -NF κ B in microglia. **A** The expression of PP2A, PKC- δ , NF- κ B p65, p-NF- κ B p65, I κ B α and p-I κ B α were detected in the mPFC using western blot. **B** The expression of PP2A, PKC- δ , NF- κ B p65, p-NF- κ B p65, I κ B α and p-I κ B α were detected in the hippocampus using western blot. **C** Semi-quantification for different proteins expression were normalized in the mPFC. **D** Semi-quantification for different proteins expression were normalized in the hippocampus. All data were presented as mean \pm SEM. * $p < 0.05$, ** $p < 0.01$, and *** $p < 0.001$; ns, not significant. For detailed statistics information, see Table S1

remains remarkably stable, because microglial proliferation in adult rodent brains is slow under physiologically healthy conditions. In contrast, microglia increase their population by both proliferation of resident microglia and recruitment of blood-derived immune cells under pathological brain conditions, for example, LPS induces systemic inflammation and disruption of the blood–brain barrier occurs. A large amount of evidence indicates that there is a causative relationship between microglial proliferation and neurocognitive outcomes. This is further confirmed by the fact that the inhibition of microglial proliferation by pharmacological inhibitors against colony stimulating factor receptor 1 (CSF1R) produced an improvement in neurocognitive deficits (Olmos-Alonso et al. 2016). Our findings suggest that C21 treatment efficiently reduces the proliferation of microglia as well as reactive microglia. Numerous efforts have recently been made to explain the molecular mechanism by which AGTR2 mitigates reactive microglia and their subsequent function. Traditionally, AGTR2 is believed to be highly expressed in the fetus but rapidly declines to an extremely low level after birth (Lenkei et al. 1996; de Kloet et al. 2016). Recently, it has been increasingly acknowledged that inducible AGTR2 expression is abundantly elicited on activated microglia in response to challenges, and AGTR2 stimulation might exert anti-inflammatory action via the inhibition of microglia, which leads to an improved outcome in neurological disease (Jackson et al. 2018; Rivas-Santisteban et al. 2021). Our findings strengthen the beneficial role of AGTR2 on neurocognitive outcome, which is linked to a reduction in reactive microglia, and microglial engulfment of the synapse. NADPH oxidase activation and subsequent ROS overproduction are important upstream events that can activate microglia and amplify microglial dysfunction (Dohi et al. 2010; Kumar et al. 2016). There are multiple sources of the production of ROS, among which the most studied include NADPH oxidase and mitochondrial ROS (Circu and Aw 2010). Despite a disagreement on the extent to which mitochondria produce ROS in vivo, NADPH oxidase is regarded as the predominant source of ROS in phagocytes such as microglia, which is upregulated in SAE and POCD and essential for microglia-mediated amyloid neurotoxicity (Bhat et al. 2019). We demonstrated here that pretreatment with C21 lessened microglial NOX2 expression and resulted in ROS production in the prefrontal cortex and hippocampus in mice subjected to LPS/MV. In addition to NOX2-derived ROS, it cannot be neglected that microglia produce a

wide spectrum of neural active substances to participate in the neuroinflammatory cascade and synaptic dysfunction, such as IL-1 and TNF as well as neuroprotective factors, including BDNF which is critically involved in synaptic maturation and plasticity (Jiang et al. 2022). Although others and our data revealed that the substantial increase in IL-1, TNF, and BDNF levels occurs concomitantly with reactive microglia, there is a limitation that we did not deeply investigate whether and how the alteration of these substances drives the subsequent neurological dysfunction. Furthermore, the findings from our and others' works have demonstrated that stimulation of AT2R induces the activation of PP2A, which is a protein phosphatase that leads to the dephosphorylation of PKC δ that typically results in the subsequent NF- κ B-mediated transcriptional activation in microglia.

Conclusions

In summary, our findings revealed that the AGTR2 agonist C21 alleviated behavioral deficits in mice subjected to LPS/MV cochallenge in a microglia-dependent manner via inhibition of aberrant reactive microglia and microglial engulfment of neuronal synapses. The findings of this study provide experimental evidence supporting the pharmacological stimulation of AGTR2 by C21 and may be valuable for the development of prevention or mitigation strategies for neurological morbidity in these critically ill patients.

Supplementary Information The online version contains supplementary material available at <https://doi.org/10.1007/s11481-022-10054-7>.

Acknowledgements The authors very much appreciate Professor Zhi Zhang for kindly providing the *Cx3cr1-GFP* and *Thy1-YFP* mice.

Authors' Contributions D. WANG, L. SHEN, and D. CHEN designed the studies, conducted most of the experiments and data analysis and wrote the draft manuscript. Q. LOU, P. CAO, and R. HU conducted the behavioral experiments and data analysis and wrote the text of the final manuscript. Y. JIN, S. HU, and D. WANG were involved in the overall design of the study and approved the final manuscript.

Funding This work was supported by the National Key Research and Development Program of China (2021ZD0203105), National Natural Science Foundation of China (81703524, 82171218), Natural Science Foundation of Anhui Province (1608085QH210), Fundamental Research Funds for the Central Universities (WK910000030), USTC Research Funds of the Double First-Class Initiative (YD9100002018), and Youth Innovation Promotion Association CAS.

Data Availability The data that support the findings of this study are available from the corresponding author (Dr. Shan-shan Hu) upon request.

Declarations

Ethics Approval and Consent to Participate This study was approved by experimental Animal Ethics Committee of Anhui Medical University (No. LLSC20160121), and all experiment protocols were approved by the Institutional Animal Care and Use Committee of Anhui Medical University.

Consent for Publication This research did not receive any specific grant from funding agencies in the public, commercial, or not-for-profit sectors.

Competing Interests The authors declare that they have no competing interests.

References

- Alhusban A, Fouda AY, Bindu P, Ishrat T, Soliman S, Fagan SC (2015) Compound 21 is pro-angiogenic in the brain and results in sustained recovery after ischemic stroke. *J Hypertens* 33:170–180
- Bhat SA, Sood A, Shukla R, Hanif K (2019) AT2R activation prevents microglia pro-inflammatory activation in a NOX-Dependent manner: inhibition of PKC activation and p47(phox) phosphorylation by PP2A. *Mol Neurobiol* 56:3005–3023
- Bhat SA, Fatima Z, Sood A, Shukla R, Hanif K (2021) The protective effects of AT2R agonist, CGP42112A, against angiotensin ii-induced oxidative stress and inflammatory response in astrocytes: role of AT2R/PP2A/NFkappaB/ROS signaling. *Neurotox Res* 39:1991–2006
- Cao P et al (2021) Early-life inflammation promotes depressive symptoms in adolescence via microglial engulfment of dendritic spines. *Neuron* 109(2573–2589):e2579
- Chen C, Zhang Z, Chen T, Peng M, Xu X, Wang Y (2015) Prolonged mechanical ventilation-induced neuroinflammation affects post-operative memory dysfunction in surgical mice. *Crit Care* 19:159
- Chen T, Chen C, Zhang Z, Zou Y, Peng M, Wang Y (2016) Toll-like receptor 4 knockout ameliorates neuroinflammation due to lung-brain interaction in mechanically ventilated mice. *Brain Behav Immun* 56:42–55
- Chen Z, Jalabi W, Shpargel KB, Farabaugh KT, Dutta R, Yin X, Kidd GJ, Bergmann CC, Stohlman SA, Trapp BD (2012) Lipopolysaccharide-induced microglial activation and neuroprotection against experimental brain injury is independent of hematogenous TLR4. *J Neurosci* 32:11706–11715
- Circu ML, Aw TY (2010) Reactive oxygen species, cellular redox systems, and apoptosis. *Free Radic Biol Med* 48:749–762
- Cobley JN, Fiorello ML, Bailey DM (2018) 13 reasons why the brain is susceptible to oxidative stress. *Redox Biol* 15:490–503
- de Kloet AD, Wang L, Ludin JA, Smith JA, Pioquinto DJ, Hiller H, Steckelings UM, Scheuer DA, Summers C, Krause EG (2016) Reporter mouse strain provides a novel look at angiotensin type-2 receptor distribution in the central nervous system. *Brain Struct Funct* 221:891–912
- Ding N, Wang F, Xiao H, Xu L, She S (2013) Mechanical ventilation enhances HMGB1 expression in an LPS-induced lung injury model. *PLoS ONE* 8:e74633
- Ding X, Tong Y, Jin S, Chen Z, Li T, Billiar TR, Pitt BR, Li Q, Zhang LM (2018) Mechanical ventilation enhances extrapulmonary sepsis-induced lung injury: role of WISP1-alpha5 integrin pathway in TLR4-mediated inflammation and injury. *Crit Care* 22:302
- Dohi K, Ohtaki H, Nakamachi T, Yofu S, Satoh K, Miyamoto K, Song D, Tsunawaki S, Shioda S, Aruga T (2010) Gp91phox (NOX2) in classically activated microglia exacerbates traumatic brain injury. *J Neuroinflammation* 7:41
- Eldahshan W, Ishrat T, Pillai B, Sayed MA, Alwhaibi A, Fouda AY, Ergul A, Fagan SC (2019) Angiotensin II type 2 receptor stimulation with compound 21 improves neurological function after stroke in female rats: a pilot study. *Am J Physiol Heart Circ Physiol* 316:H1192–H1201
- Ely EW, Shintani A, Truman B, Speroff T, Gordon SM, Harrell FE Jr, Inouye SK, Bernard GR, Dittus RS (2004) Delirium as a predictor of mortality in mechanically ventilated patients in the intensive care unit. *JAMA* 291:1753–1762
- Furube E, Kawai S, Inagaki H, Takagi S, Miyata S (2018) Brain Region-dependent Heterogeneity and Dose-dependent Difference in Transient Microglia Population Increase during Lipopolysaccharide-induced Inflammation. *Sci Rep* 8:2203
- Giordano G, Pugliese F, Bilotta F (2021) Neuroinflammation, neuronal damage or cognitive impairment associated with mechanical ventilation: a systematic review of evidence from animal studies. *J Crit Care* 62:246–255
- Gofton TE, Young GB (2012) Sepsis-associated encephalopathy. *Nat Rev Neurol* 8:557–566
- Helms J, Kremer S, Merdji H, Clere-Jehl R, Schenck M, Kummerlen C, Collange O, Boulay C, Fafi-Kremer S, Ohana M, Anheim M, Meziani F (2020) Neurologic features in severe SARS-CoV-2 infection. *N Engl J Med* 382:2268–2270
- Hoogland IC, Houbolt C, van Westerloo DJ, van Gool WA, van de Beek D (2015) Systemic inflammation and microglial activation: systematic review of animal experiments. *J Neuroinflammation* 12:114
- Huang WY, Liu KH, Lin S, Chen TY, Tseng CY, Chen HY, Wu HM, Hsu KS (2020) NADPH oxidase 2 as a potential therapeutic target for protection against cognitive deficits following systemic inflammation in mice. *Brain Behav Immun* 84:242–252
- Jackson-Cowan L, Eldahshan W, Dumanli S, Dong G, Jamil S, Abdul Y, Althomali W, Baban B, Fagan SC, Ergul A (2021) Delayed Administration of Angiotensin Receptor (AT2R) agonist C21 improves survival and preserves sensorimotor outcomes in female diabetic rats post-stroke through modulation of microglial activation. *Int J Mol Sci* 22:1356
- Jackson L, Eldahshan W, Fagan SC, Ergul A (2018) Within the Brain: The Renin Angiotensin System. *Int J Mol Sci* 19:876
- Jackson L, Dong G, Althomali W, Sayed MA, Eldahshan W, Baban B, Johnson MH, Filosa J, Fagan SC, Ergul A (2020) Delayed administration of angiotensin II type 2 receptor (AT2R) agonist compound 21 prevents the development of post-stroke cognitive impairment in diabetes through the modulation of microglia polarization. *Transl Stroke Res* 11:762–775
- Jiang J, Tang B, Wang L, Huo Q, Tan S, Misrani A, Han Y, Li H, Hu H, Wang J, Cheng T, Tabassum S, Chen M, Xie W, Long C, Yang L (2022) Systemic LPS-induced microglial activation results in increased GABAergic tone: a mechanism of protection against neuroinflammation in the medial prefrontal cortex in mice. *Brain Behav Immun* 99:53–69
- Jing F, Mogi M, Sakata A, Iwanami J, Tsukuda K, Ohshima K, Min LJ, Steckelings UM, Unger T, Dahlof B, Horiuchi M (2012) Direct stimulation of angiotensin II type 2 receptor enhances spatial memory. *J Cereb Blood Flow Metab* 32:248–255
- Kang HJ, Voleti B, Hajszan T, Rajkowska G, Stockmeier CA, Licznarski P, Lepack A, Majik MS, Jeong LS, Banasr M, Son H, Duman RS (2012) Decreased expression of synapse-related genes and loss of synapses in major depressive disorder. *Nat Med* 18:1413–1417
- Kumar A, Barrett JP, Alvarez-Croda DM, Stoica BA, Faden AI, Loane DJ (2016) NOX2 drives M1-like microglial/macrophage activation and neurodegeneration following experimental traumatic brain injury. *Brain Behav Immun* 58:291–309
- Lenkei Z, Palkovits M, Corvol P, Llorens-Cortes C (1996) Distribution of angiotensin II type-2 receptor (AT2) mRNA expression in the adult rat brain. *J Comp Neurol* 373:322–339
- Liu Z, Yao X, Jiang W, Li W, Zhu S, Liao C, Zou L, Ding R, Chen J (2020) Advanced oxidation protein products induce microglia-mediated neuroinflammation via MAPKs-NF-kappaB signaling pathway and pyroptosis after secondary spinal cord injury. *J Neuroinflammation* 17:90
- Manabe T, Heneka MT (2022) Cerebral dysfunctions caused by sepsis during ageing. *Nat Rev Immunol* 22:444–458

- Mei B, Li J, Zuo Z (2021) Dexmedetomidine attenuates sepsis-associated inflammation and encephalopathy via central alpha2A adrenoceptor. *Brain Behav Immun* 91:296–314
- Olmos-Alonso A, Schettters ST, Sri S, Askew K, Mancuso R, Vargas-Caballero M, Holscher C, Perry VH, Gomez-Nicola D (2016) Pharmacological targeting of CSF1R inhibits microglial proliferation and prevents the progression of Alzheimer's-like pathology. *Brain* 139:891–907
- Pan TT, Gao W, Song ZH, Long DD, Cao P, Hu R, Chen DY, Zhou WJ, Jin Y, Hu SS, Wei W, Chai XQ, Zhang Z, Wang D (2022) Glutamatergic neurons and myeloid cells in the anterior cingulate cortex mediate secondary hyperalgesia in chronic joint inflammatory pain. *Brain Behav Immun* 101:62–77
- Pandharipande PP, Girard TD, Jackson JC, Morandi A, Thompson JL, Pun BT, Brummel NE, Hughes CG, Vasilevskis EE, Shintani AK, Moons KG, Geevarghese SK, Canonico A, Hopkins RO, Bernard GR, Dittus RS, Ely EW, Investigators B-IS (2013) Long-term cognitive impairment after critical illness. *N Engl J Med* 369:1306–1316
- Pun BT et al (2021) Prevalence and risk factors for delirium in critically ill patients with COVID-19 (COVID-D): a multicentre cohort study. *Lancet Respir Med* 9:239–250
- Qiu LL, Ji MH, Zhang H, Yang JJ, Sun XR, Tang H, Wang J, Liu WX, Yang JJ (2016) NADPH oxidase 2-derived reactive oxygen species in the hippocampus might contribute to microglial activation in postoperative cognitive dysfunction in aged mice. *Brain Behav Immun* 51:109–118
- Rivas-Santesteban R, Lillo J, Munoz A, Rodriguez-Perez AI, Labandeira-Garcia JL, Navarro G, Franco R (2021) Novel interactions involving the mas receptor show potential of the renin-angiotensin system in the regulation of microglia activation: altered expression in parkinsonism and dyskinesia. *Neurotherapeutics* 18:998–1016
- Royea J, Lacalle-Aurioles M, Trigiani LJ, Fermigier A, Hamel E (2020) AT2R's (Angiotensin II Type 2 Receptor's) role in cognitive and cerebrovascular deficits in a mouse model of Alzheimer disease. *Hypertension* 75:1464–1474
- Saito M, Fujinami Y, Ono Y, Ohyama S, Fujioka K, Yamashita K, Inoue S, Kotani J (2021) Infiltrated regulatory T cells and Th2 cells in the brain contribute to attenuation of sepsis-associated encephalopathy and alleviation of mental impairments in mice with polymicrobial sepsis. *Brain Behav Immun* 92:25–38
- Sasanejad C, Ely EW, Lahiri S (2019) Long-term cognitive impairment after acute respiratory distress syndrome: a review of clinical impact and pathophysiological mechanisms. *Crit Care* 23:352
- Schwengel K, Namsolleck P, Lucht K, Clausen BH, Lambertsen KL, Valero-Esquitino V, Thone-Reineke C, Muller S, Widdop RE, Denton KM, Horiuchi M, Iwai M, Boato F, Dahlof B, Hallberg A, Unger T, Steckelings UM (2016) Angiotensin AT2-receptor stimulation improves survival and neurological outcome after experimental stroke in mice. *J Mol Med (berl)* 94:957–966
- Slutsky AS, Tremblay LN (1998) Multiple system organ failure. Is mechanical ventilation a contributing factor? *Am J Respir Crit Care Med* 157:1721–1725
- Sparrow NA, Anwar F, Covarrubias AE, Rajput PS, Rashid MH, Nisnon PL, Gezalain MM, Toossi S, Ayodele MO, Karumanchi SA, Ely EW, Lahiri S (2021) IL-6 inhibition reduces neuronal injury in a murine model of ventilator-induced lung injury. *Am J Respir Cell Mol Biol* 65:403–412
- Terrando N, Rei Fidalgo A, Vizcaychipi M, Cibelli M, Ma D, Monaco C, Feldmann M, Maze M (2010) The impact of IL-1 modulation on the development of lipopolysaccharide-induced cognitive dysfunction. *Crit Care* 14:R88
- Tonnies E, Trushina E (2017) Oxidative stress, synaptic dysfunction, and Alzheimer's disease. *J Alzheimers Dis* 57:1105–1121
- Turon M, Fernandez-Gonzalo S, de Haro C, Magrans R, Lopez-Aguilar J, Blanch L (2018) Mechanisms involved in brain dysfunction in mechanically ventilated critically ill patients: implications and therapeutics. *Ann Transl Med* 6:30
- Wang C, Yue H, Hu Z, Shen Y, Ma J, Li J, Wang XD, Wang L, Sun B, Shi P, Wang L, Gu Y (2020) Microglia mediate forgetting via complement-dependent synaptic elimination. *Science* 367:688–694
- Wen J, Ribeiro R, Zhang Y (2011) Specific PKC isoforms regulate LPS-stimulated iNOS induction in murine microglial cells. *J Neuroinflammation* 8:38
- Werneburg S, Jung J, Kunjamma RB, Ha SK, Luciano NJ, Willis CM, Gao G, Biscola NP, Havton LA, Crocker SJ, Popko B, Reich DS, Schafer DP (2020) Targeted complement inhibition at synapses prevents microglial synaptic engulfment and synapse loss in demyelinating disease. *Immunity* 52(167–182):e167
- Wilcox ME, Brummel NE, Archer K, Ely EW, Jackson JC, Hopkins RO (2013) Cognitive dysfunction in ICU patients: risk factors, predictors, and rehabilitation interventions. *Crit Care Med* 41:S81–98
- Zhang B, Bailey WM, McVicar AL, Stewart AN, Veldhorst AK, Gensel JC (2019) Reducing age-dependent monocyte-derived macrophage activation contributes to the therapeutic efficacy of NADPH oxidase inhibition in spinal cord injury. *Brain Behav Immun* 76:139–150
- Zhang C, Hu S, Zosky GR, Wei X, Shu S, Wang D, Chai X (2021) Paradoxib alleviates ventilator-induced lung injury through functional modulation of lung-recruited CD11b/LoLy6Chi monocytes. *Shock* 55:236–243

Publisher's Note Springer Nature remains neutral with regard to jurisdictional claims in published maps and institutional affiliations.

Springer Nature or its licensor (e.g. a society or other partner) holds exclusive rights to this article under a publishing agreement with the author(s) or other rightsholder(s); author self-archiving of the accepted manuscript version of this article is solely governed by the terms of such publishing agreement and applicable law.